

Assessing the linear and planer micro-structural defects in SnO₂ Nanoparticles through high resolution transmission electron microscopy (HRTEM)

Shrabani Mondal¹, Rashmi Madhuri², Prashant K. Sharma^{1*}

¹ Functional Nanomaterials Research Laboratory, Department of Applied Physics, Indian Institute of Technology (ISM), Dhanbad-826004, India

² Department of Applied Chemistry, Indian Institute of Technology (ISM), Dhanbad-826004, India

*Corresponding author: E-mail:prashantnac@gmail.com

Received: 03 April 2017, Revised: 05 April 2017 and Accepted: 09 April 2017

DOI: 10.5185/amlett.2017.1741

www.vbripress.com/aml

Abstract

This letter assesses the origin of linear and planer micro-structural defects in SnO₂ nanoparticles through high resolution transmission electron microscopy (HRTEM). For the purpose, SnO₂ nanoparticles of size 5-15 nm are synthesized by chemical co-precipitation followed by calcinations. In the low temperature (200°C and 400°C) calcinations range no significant evidence of micro-structural defect are observed. Whereas, SnO₂ nanoparticles calcined at 600°C shows better crystallinity with multiple 1-D linear defects along with 2-D planer defects. Contribution of size and strain effect causing such circumstances is illustrated in detail. Influence of these micro-structural defects on the luminescence properties of SnO₂ nanoparticles is also elaborated in detail. Copyright © 2017 VBRI Press.

Keywords: SnO₂ nanoparticles, defects, strain, high resolution transmission electron microscopy, photoluminescence.

Introduction

Nanostructured SnO₂ has gained special interest owing to its unique optoelectronic and catalytic properties. Size dependent flexible properties (e.g. quantum confinement effect) are the especial feature of nanomaterials which distinguish them from their bulk counterparts [1]. Tunable fundamental properties; electronic structure, phase stability etc., are determined during the process of crystal growth [2, 3]. Hence, the understanding of growth factors, viz. strain, reaction kinetics and microstructure, are necessary to control the material properties at nanoregime [4]. So far, huge efforts have been devoted in preparation and characterizations of SnO₂ to improve its features and extend the applicability [5, 6]. However, the analysis of microstructural defects inside the nanoparticles and their influences are still unclear. As, the microstructure and physical properties of material is strongly co-related [7], microstructural information is crucial to acquire. Numerous reports show that the strength, ductility, elasticity, color center can be tailored up to a considerable mark by controlling defects [8, 9]. During nanoparticles formation, specific defects can be introduced by varying preparation conditions and hence the properties of the materials can be tailored accordingly.

Ostwald ripening (OR) process is described as key factor affecting the nanoparticle formation. According to OR model, crystal growth takes place through diffusion of atoms and the growth kinetics depends on the nature of solution, solution-crystal interface and material structure [10, 11]. So, OR model is suitable for all length scale, as the aforementioned parameters are independent of crystal size [12]. Other than OR, in some cases [13] oriented attachment (OA) based crystal growth is also reported. Initially in this process, formation of bigger particle from seed particles occur when adjacent smaller particles of different orientation coalesce to share a common crystal plane by eliminating their interfaces [12]. Planer and linear defects in coalesced particles are the byproducts of OA based crystal growth [13].

Earlier, Wang *et al.* had produced single, double and multiple nanotwins in Silicon (Si) nanocrystals by ion implantation of Si into SiO₂ film and related the PL intensity with planer defects [9]. Evolution of structural defects and strain effect in Germanium (Ge) nanocrystals deposited onto SiO₂ films was performed by Zhang *et al.* [14]. Ding *et al.* had reported formation mechanism of pure edge dislocations (parallel and perpendicular) at the BMCO/STO interface in order to understand the

microstructure dependent physical properties of materials [7].

To the best of our knowledge, study on crystal defects with respect to calcination temperature on SnO₂ nanoparticles and their influences on optical properties has not been explored yet. Herein, we report the HRTEM analysis of micro-structural defects in SnO₂ nanoparticles during crystal growth governed by OA method. Relation of defect concentration with calcination temperature is explained considering the consequences of size and residual strain. Linear defect (dislocation) and planer defects namely stacking faults (SF) and twins are clearly evident. Origin and formation mechanisms of these defects are discussed in detail. The influence of these micro-structural defects on the luminescence properties of SnO₂ nanoparticles with respect to crystallite size and microstructure is also elaborated.

Experimental:

Materials details

Stannic chloride (SnCl₄ · 5H₂O) and ammonia solution were purchased from Fischer Scientific, India, and was used as purchased without any further purification. Double distilled water was used throughout the experiments.

Material synthesis

In a simple co-precipitation procedure, 0.2 M Stannic chloride was dissolved in 100 mL of double distilled water under continuous stirring until a transparent solution was obtained. In the next step, ammonia solution (98%) was added drop wise under vigorous stirring to increase the solution pH up to 5. At this pH, the transparent solution became turbid. The stirring was allowed for further 2 h. Finally, obtained white slurry was centrifuged at 4500 rpm for 15 min followed by the washing with distilled water and ethanol repeatedly. Washing was continued till the ammonium ion was traced by aqueous sodium hydroxide. The filtrate was dried at 50°C for 3 h in hot air oven and then allowed to cool at room temperature naturally. The yielded white product was subsequently divided into three equal parts and then transferred to a muffle furnace at different temperatures viz. 200°C, 400°C, 600°C. Finally, the calcined samples were grinded using agate mortar and collected for various characterizations.

Characterizations

Crystal structure of the powder samples were examined and confirmed via Brüker D8 powder X-ray diffractometer, USA, using CuK α ($\lambda = 1.5406 \text{ \AA}$) radiation as X-ray source. TEM and HRTEM images were captured using Tecnai 30 G² S-Twin electron microscope (FEI Co. Netherlands), operated at 300 kV. Photoluminescence spectra were recorded on LS 55 Perkin Elmer Spectrophotometer, USA, with 375 nm excitation

wavelength. An amount of 0.5g powder sample was used for PL measurements.

Results and discussion

The XRD patterns of the samples calcined at different temperature are presented in **Fig. 1a**. Diffraction peaks obtained at 2θ values; 26.9°, 34.4°, 38.5°, 52.3°, 55.16°, 58.2°, 62.3°, 64.9°, 66.3°, 71.6°, 79.15° are in excellent agreement with JCPDS/ICDD card no 88-0287, and can be indexed as tetragonal lattice having space group P4₂/mmm. Broad peaks in 200°C calcined sample indicates the amorphous nature of the sample with very small sized particles. However, rise in temperature result more intense diffraction peaks with less broadening, suggest the generation of larger crystallites. The average crystallite size of the samples calcined at 200, 400 and 600°C are calculated using Scherrer formula [15] and are found to be 2 nm, 4 nm and 12 nm respectively.

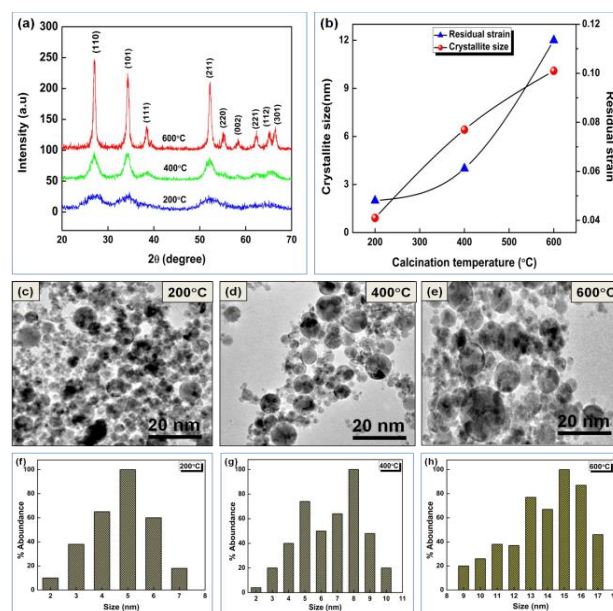


Fig.1. (a) XRD patterns of SnO₂ samples calcined at different temperatures. (b) Variation of crystallite size and strain with calcination temperature. (c)-(e) and (f)-(g) Show the TEM images and distribution of particle size at different calcination temperature, 200, 400 and 600°C respectively.

From precise analysis of TEM images (**Fig. 1(c)-(d)**), the particle size distribution of all the samples is measured using the Image-J software against randomly selected 50 particles. The histograms are plotted in **Fig. 1(f)-(h)**. This increasing trend of particle size with calcination temperature is due to the coalescence of small nanocrystals during thermal treatment. This observation is similar to the previously observed results in case of Ge nanocrystals [16, 17]. Here it is to be mentioned that, the size calculated from Scherrer equation (from XRD) and measured from TEM images are not consistent which is obvious. Scherrer equation gives the size of the crystallites [15] whereas from TEM image we can measure the particle size. Generally, particle size and

crystallite size is not the same thing [4], and one particle can be composed by the aggregation of several crystallites.

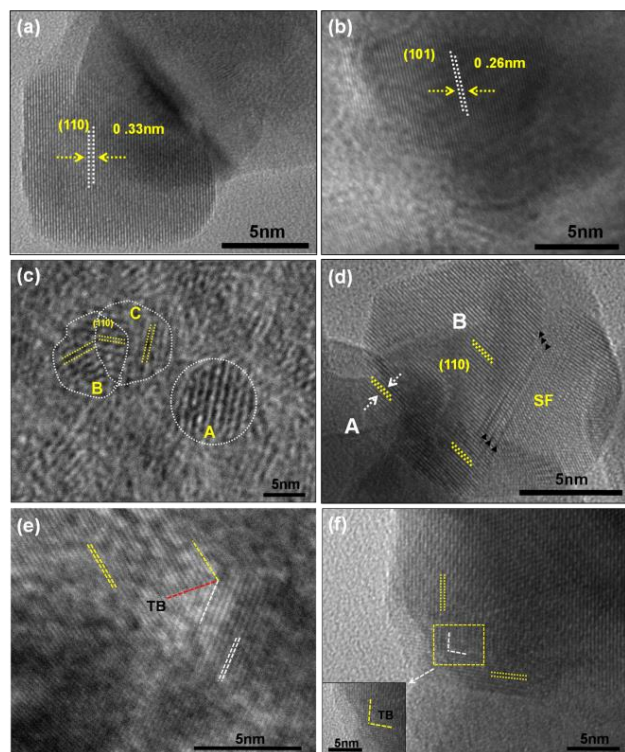


Fig. 2. Typical HRTEM images of sample calcined at (a) 200°C and (b) 400°C. HRTEM images of sample calcined at 600°C, (c) An individual SnO₂ nanoparticle and two particles with different orientations about to combine together along preferred orientation, (d) Stacking faults, (e) and (f) twinning structures.

High resolution TEM images indicate the presence of variety of microstructural defects, 1-dimensional linear (dislocations) defects and 2-dimensional planer defects, namely twin and stacking faults. In present case, microstructural defects are predominantly observed in SnO₂ sample calcined at 600°C whereas other two samples prepared at 200°C and 400°C show regular lattice patterns with significantly small defect zones [Fig. 2(a)-(b)]. The reason may be attributed to the size and strain effect [18]. According to previously reported results linear defect concentration is strongly related to the crystallite size and below a critical size the existence of dislocations is virtually zero [18, 19]. Also, planer defects are commonly formed in bigger nanoparticles [14]. Perhaps the smaller size of nanoparticles (<10nm) formed after calcination at 200°C and 400°C has minimized the formation of such 2-D defects. To further understand the relation between defect concentrations with residual strain, we have estimated the strain value using W-H plot for all calcined samples. The obtained values are 0.041, 0.077 and 0.101 for the samples prepared at 200, 400 and 600°C, respectively. Hence, it is clear that this increasing nature of residual strain is related to the calcination temperature as well as the size of particles [Fig. 1(b)]. During crystallization process,

contribution of volume contraction in residual strain is smaller and elasticity can manage the strain easily [14]. Also, because of the higher surface area to volume ratio, smaller nanoparticles possess higher surface energy. Hence, these high energy defects are incompatible with the total energy of smaller nanoparticles [9]. They can move smoothly through the smaller nanoparticle and vanish [9]. Hence the defects are avoided in smaller particles. But in such scenario, formation of defects in bigger nanoparticles provides an effective way to release the accumulated energy of strain fields during nanoparticles growth [14].

For the SnO₂ sample calcined at 600°C, presences of dislocations are appreciably higher than planer defects. Rise in temperature increases the frequency of coalescence of smaller nanoparticles and promotes the formation of dislocations in order to relax the stress field [14]. Few twinning structures are also observed in the vicinity region of the dislocations which are also resulted from the coalesced particles. Under certain conditions, if the internal stress field still remains, the excess energy releases in terms of twins. Wang *et al.* had observed this phenomenon in Si crystals previously [9]. In Fig. 2(c), A is an individual nanocrystal of SnO₂, B and C are two nanocrystals with different orientations which are about to coalesce at their interface along a preferred orientation. In coalescence/OA process, nanoparticles themselves play the role of building blocks for crystal growth [20]. These types of combined nanoparticles are frequently noticed throughout the sample. Coalescence of smaller nanocrystals into a bigger one is very favorable during thermal treatment in order to minimize the total energy of the system [14]. Since, the surface area of combined nanocrystals are much smaller than the other isolated nanoparticles, the energy minimization effect is satisfied [14]. (110) plane of tetragonal SnO₂ is energetically favorable. So, initially smaller nanoparticles tend to orient along (110) face during coalescence process. Similar phenomenon is already observed in cubic closed packed Ge crystals [14] and also in Si crystals [20]. Fig. 2(d) shows an example of isolated nanoparticle formed after coalescence with stacking fault, where the orientation is along (110) direction. The size of the nanoparticle is around 14 nm. Fig. 2(e), (f) shows typical HR-TEM image of nanoparticles with single-twinning structure. Either side of the nanotwin configuration is labeled using the yellow, white lines to highlight the consisting planes and the twin boundary is denoted by red line. Careful examination indicates, dislocations, twins and stacking faults coexists in these SnO₂ nanoparticles. The reason may be attributed to the release of excessive energy during the reorganization and alignment process of atoms along lattice planes [21]. Dislocation lines are defined as the directions along which the regular crystal symmetry is lost. The area which is appreciably disturbed due to the presence of dislocation line is called dislocation core (DC). As an example of the coexistence of planer and linear defect, HRTEM image of such nanoparticles are shown in Fig. 3. Several defect regions, according to their distinguished natures, are indexed in the image. Distinct

particles have same orientations of lattice plane. Minute observation of lattice fringe indicates the aggregation of a number of primary particles having different orientations. Each region (primary particle) is distinguished by letters (A-F) for clarity and the dislocation regions are highlighted by white circles named as DC. Stacking faults are pointed out by black arrows named as SF, and twins by yellow bent lines labeled with TB. At the interface of A-B and B-E two linear defects are found. At interface of A-F, B-D and C-E are twins. Interestingly, we found that most of the stacking faults are located at the core of particle, whereas, twins and dislocations are created at the interface of the primary particles. The reason can be attributed to the energy optimization effect at the interfaces of primary nanoparticles [20]. A detail analysis on this aspect is still to be explored.

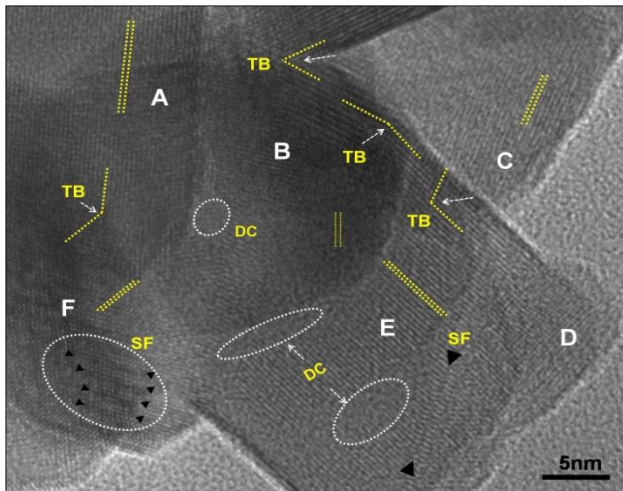


Fig. 3. HRTEM image of a typical SnO₂ nanoparticle calcined at 600°C with various planer and linear defects.

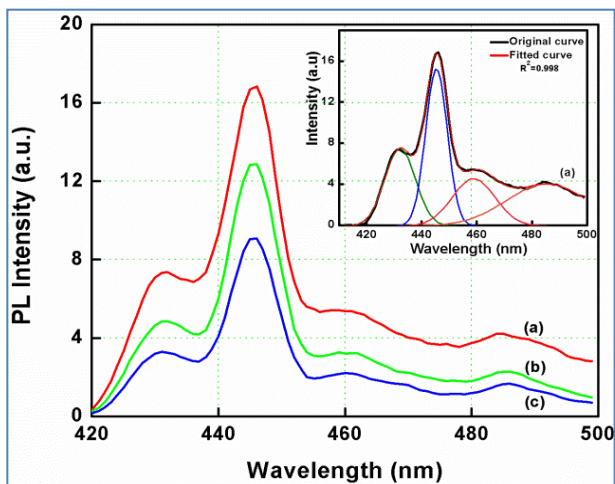


Fig. 4. PL spectra obtained from the SnO₂ samples calcined at (a) 200°C, (b) 400°C and (c) 600°C. Inset shows the de-convoluted spectrum of SnO₂ nanoparticles prepared at 200°C.

Owing to the wide band gap (3.6 eV) and high exciton binding energy (130 meV), SnO₂ acquire a special attention in the optoelectronic applications [22]. However,

excitonic emission intensity can be tailored by controlling the size of the nanostructured SnO₂ [22]. It is well established that, change in size affects the defect states; viz. oxygen vacancies, dangling bonds etc. [22]. Hence, in order to improve the effectiveness of the optoelectronic device, emission efficiency of the material is to be optimized. PL gives a better understanding about the defect levels associated with any material and also helps to recognize additional defects created by any modification of the particular material [23].

In order to observe the influence of defects in present case, we have recorded room temperature PL spectra (shown in Fig. 4) of all the samples at excitation wavelength 375 nm. For better clarity of emission peaks, one de-convoluted spectra using Gaussian fitting with a fitted value of 0.998 is demonstrated in the inset. Four prominent peaks positioned at 433, 445, 458 and 485 nm are observed in each case with the maximum intense peak centered at 445 nm. The origin of these peaks is already well explained in literature [24-26]. Oxygen vacancies are considered as major contributors in PL emission by recombining with an electron in oxide materials [27]. In brief, 433 nm emission is ascribed to the tin interstitials, 445 nm and 458 nm emissions are generated by the radiative recombination of doubly ionized oxygen vacancies (V_o^{++}) [24, 25]. 485 nm emission is due to the singly ionized oxygen vacancies (V_o^+) located at the nanoparticle surface [26]. The objective of the present work is to understand the effect of extended defects (dislocations) on the observed optical behavior. According to Albrecht *et al.*, high strain and intrinsic defects like dislocations usually act as nonradiative recombination centre quenching the emissions in semiconductors [28]. Hence, the intensity reduction in present case gives direct indication about the formation of intrinsic microstructural defects which occurs with calcination temperature. In n-type materials, the dangling bonds formed due to the dislocation behave like acceptors and are able to trap electrons. This negatively charged dislocation lines serve as columbic scattering centre which restricts the electron transportation and quenches the PL intensity [29]. In n-type AlGaIn, edge dislocation is inferred as the major reason for the severe decrease in PL intensity [29]. SnO₂ sample calcined at 600°C possess minimum PL intensity because of the presence of larger amount of dislocations.

Conclusion

We have studied the microstructural features of chemically synthesized SnO₂ nanoparticles of 5-15 nm size. Crystal growth process by coalescence is explained using oriented attachment model. It has been found that, at high temperature, 600°C, effective growth of SnO₂ nanoparticle occurs showing better crystallinity with several linear and planer defects. A description concerning the effect of crystallite size and residual strain with microstructural defects is provided in this work. It also gives an understanding about the relationship of dislocations with PL intensity. The present work infers

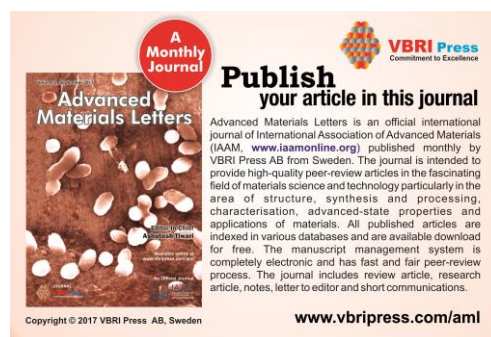
the underlying relation of emission efficiency and defects which will help in engineering the SnO₂ based optoelectronic devices.

Acknowledgements

Authors are thankful to Department of Science and Technology, Government of India for sanction of Fast Track Research Project for Young Scientists to Dr. Prashant K. Sharma (Ref. No.: SR/FTP/PS-157/2011) and Dr. Rashmi Madhuri (Ref. No.: SB/FT/CS-155/2012). Dr. Sharma (FRS/34/2012-2013/APH) and Dr. Madhuri (FRS/43/2013-2014/AC) are also thankful to Indian Institute of Technology (ISM), Dhanbad for grant of Major Research Project under Faculty Research Scheme. We are also thankful to Board of Research in Nuclear Sciences (BRNS), Department of Atomic Energy, Government of India for major research project (Sanction No. 34/14/21/2014-BRNS/0295). Authors also sincerely acknowledge the facilities available in Central Research Facility of the Institute. Ms. Shrabani is also thankful to Indian Institute of Technology (ISM), Dhanbad for Senior Research Fellowship.

References

- Sharma, P.K.; Pandey, A.C.; Zolnierkiewicz, G.; Guskos, N.; Rudowicz, C; *J. Appl. Phys.*, **2009**, *106*, 094314.
DOI: [10.1063/1.3256000](https://doi.org/10.1063/1.3256000)
- Alivisatos, A.P; *J. Phys. Chem.*, **1996**, *100*, 13226.
DOI: [10.1021/jp9535506](https://doi.org/10.1021/jp9535506)
- Sharma, P.K.; Dutta, R.K.; Pandey, A.C.; Liu C.H.; Pandey, R; *Mat. Lett.*, **2010**, *64*, 1183.
DOI: [10.1016/j.matlet.2010.02.045](https://doi.org/10.1016/j.matlet.2010.02.045)
- Sharma, P.K.; Dutta, R.K.; Choudhary R.J.; Pandey, A.C; *Cryst. Eng. Comm.*, **2013**, *15*, 4438.
DOI: [10.1016/j.matlet.2010.02.045](https://doi.org/10.1016/j.matlet.2010.02.045)
- Pan, S.S.; Xu, J.M.; Yu, S.F.; Li, G.H.; Zhang, Y.X.; Luo, Y.Y.; Wang, S; *J. Appl. Phys.*, **2013**, *113*, 143104.
DOI: [10.1063/1.4800896](https://doi.org/10.1063/1.4800896)
- Adhikari, R.; Das, A.K; Karmakar, D.; Chanrasekhar Rao, T.V.; Ghatak, J; *Phys. Rev. B.*, **2008**, *78*, 024404.
DOI: [10.1103/PhysRevB.78.024404](https://doi.org/10.1103/PhysRevB.78.024404)
- Ding, Y.H.; Cai, R.S.; Wang, Y.Q.; Chen, Y.Z.; Sun, J.R; *Mater. Lett.*, **2012**, *67*, 67.
DOI: [10.1016/j.matlet.2011.09.026](https://doi.org/10.1016/j.matlet.2011.09.026)
- Wurschum, R.; Herth, S.; Brossmann, U; *U. Adv. Eng. Mater.*, **2003**, *5*, 365.
DOI: [10.1002/adem.200310079](https://doi.org/10.1002/adem.200310079)
- Wang, Y.Q.; Smirani, R.; Ross, G.G; *Nano. Let.*, **2004**, *4*, 2041.
DOI: [10.1021/nl048764q](https://doi.org/10.1021/nl048764q)
- Lu, K; *Mater. Sci. Eng.*, **1996**, *R16*, 161.
- Wagner, C.Z; *Elektrochem.*, **1961**, *65*, 581.
DOI: [10.1021/j100829a511](https://doi.org/10.1021/j100829a511)
- Huang, F.; Zhang, H.; Banfield, J.F; *J. Phys. Chem. B.*, **2003**, *107*, 10470.
DOI: [10.1021/jp035518e](https://doi.org/10.1021/jp035518e)
- Penn, R.L.; Banfield, J.F; *Science.*, **1998**, *281*, 969.
DOI: [10.1126/science.281.5379.969](https://doi.org/10.1126/science.281.5379.969)
- Zhang, M.; Ross, G.G.; Cai, R.; Barba, D.; Zhang, Y.; Wang, C.; Wang, Y; *Mater. Charact.*, **2014**, *93*, 1.
DOI: [10.1016/j.matchar.2014.03.010](https://doi.org/10.1016/j.matchar.2014.03.010) [1044-5803](https://doi.org/10.1044-5803)
- Patterson, A.L; *Phys. Rev.*, **1939**, *56*, 978.
DOI: [10.1103/PhysRev.56.978](https://doi.org/10.1103/PhysRev.56.978)
- Zhu, J.G.; White, C.W.; Budai, J.D.; Withrow, S.P.; Chen, Y; *J. Appl. Phys.*, **1995**, *78*, 4386.
DOI: [10.1063/10/japiau.1.359843](https://doi.org/10.1063/10/japiau.1.359843)
- Wu, X.L.; Gao, T.; Bao, X.M.; Yan, F.; Jiang, S.S.; Feng, D; *J. Appl. Phys.*, **1997**, *82*, 2704.
DOI: [10.1063/1.366089](https://doi.org/10.1063/1.366089)
- Gryaznov, V.G.; Polonsky, I.A.; Romanov, A.E.; Trusov, L.I; *Phys. Rev. B.*, **1991**, *44*, 42.
DOI: [10.1103/PhysRevB.44.42](https://doi.org/10.1103/PhysRevB.44.42)
- Narayan, J; *J. Appl. Phys.*, **2006**, *100*, 034309.
DOI: [10.1063/1.2220472](https://doi.org/10.1063/1.2220472)
- Wang, Y.; Smirani, R.; Ross, G.G.; Schiettekatte, F; *Phys. Rev. B.*, **2005**, *71*, 161310R.
DOI: [10.1103/PhysRevB.71.161310](https://doi.org/10.1103/PhysRevB.71.161310)
- Jose, J.M., Gutierrez, W.C.; Miki, M.; Yang, D.Q.; Piyakis, K.; Sacher, E; *J. Phys. Chem. B.*, **2005**, *109*, 9703.
DOI: [10.1021/jp0509459](https://doi.org/10.1021/jp0509459)
- Pan, S.S.; Li, G.H.; Pat. *Nanotechnol.*, **2011**, *5*, 138.
DOI: [10.2174/187221011795909161](https://doi.org/10.2174/187221011795909161)
- Rani, S.; Roy, S.C.; Karar, N.; Bhatnagar, M.C; *Solid. State. Commun.*, **2007**, *141*, 214.
DOI: [10.1016/j.ssc.2006.10.036](https://doi.org/10.1016/j.ssc.2006.10.036)
- Gu, F.; Wang, S.F.; Lu, M.K.; Cheng, X.F.; Liu, S.F.; Zhou, G.J.; Xu, D.; Yuan, D.R; *J. Cryst. Growth.*, **2004**, *262*, 182.
DOI: [10.1016/j.jcrysgro.2003.10.028](https://doi.org/10.1016/j.jcrysgro.2003.10.028)
- Sakurai, Y; *J. Non-Cryst. Solids.*, **2006**, *352*, 5391.
DOI: [10.1016/j.jnoncrsol.2006.08.018](https://doi.org/10.1016/j.jnoncrsol.2006.08.018)
- Fu, X.; Zhang, H.; Niu, S.; Xin, Q; *J. Solid. State. Chem.*, **2005**, *178*, 603.
DOI: [10.1016/j.jssc.2004.11.003](https://doi.org/10.1016/j.jssc.2004.11.003)
- Vanheusden, K.; Warren, W.L.; Seager, C.H.; Tallant, D.R.; Voigt, J.A.; Gnade, B.E; *J. Appl. Phys.*, **1996**, *79*, 7983.
DOI: [10.1063/1.1645312](https://doi.org/10.1063/1.1645312)
- Albrecht, M.; Weyher, J.L.; Lucznik, B.; Grzegory, I.; Porowski, S; *Appl. Phys. Lett.*, **2008**, *92*, 231909.
DOI: [10.1063/1.2928226](https://doi.org/10.1063/1.2928226)
- Chen, K.X.; Dai, Q.; Lee, W.; Kim, J.K.; Schubert, E.F.; Grandusky, J.; Mendrick, M.; Li, X.; Smart, J.A; *Appl. Phys. Lett.*, **2008**, *93*, 192108.
DOI: [10.1063/1.4812642](https://doi.org/10.1063/1.4812642)



A Monthly Journal

Publish your article in this journal

Advanced Materials Letters is an official international journal of International Association of Advanced Materials (IAAM, www.iaamonline.org) published monthly by VBRI Press AB from Sweden. The journal is intended to provide high-quality peer-review articles in the fascinating field of materials science and technology particularly in the area of structure, synthesis and processing, characterisation, advanced-state properties and applications of materials. All published articles are indexed in various databases and are available download for free. The manuscript management system is completely electronic and has fast and fair peer-review process. The journal includes review article, research article, notes, letter to editor and short communications.

Copyright © 2017 VBRI Press AB, Sweden www.vbripress.com/aml